Progress In Electromagnetics Research B, Vol. 91, 79–96, 2021

An Efficient Approximation of Frequency and Temperature-Dependent Dielectric Properties of Tissues

Mykola Zhuk* **and Jonathan Paradis**

Abstract—We here present a bivariate Chebyshev series method for the approximation of the experimental frequency and temperature dependent dielectric functions of materials. Within the framework of this method, the dielectric properties are modeled as a low-degree polynomial of the temperature variable (T), the coefficients of which have a frequency (variable f) dependency. This model is then rephrased in terms of the temperature coefficients which are given here as the rational functions of frequency. The principal merits of this method are that it produces a near-best polynomial approximation to the target function, rapidly improves with the order of approximation, and is easy to compute. The favorable features of our approach are demonstrated by considering the experimental wideband Cole-Cole models of animal tissues with the temperature-dependent parameters. The numerical results show the inferiority of the commonly used power-of-f representation of the polynomials concerned due to large rounding errors when the frequency range is large. This problem is ameliorated by expressing the appertaining coefficients as polynomials in the transformed frequency variable $x(f)$ in the Chebyshev basis. Areas of application of the results of this article include the modeling of human exposure to radiofrequency fields, development of treatment and diagnostic procedures, and food processing technologies.

1. INTRODUCTION

The knowledge of dielectric properties of biological tissues is essential in many research and industrial contexts, such as modeling human exposure to electromagnetic (EM) fields [1–3], developing treatment [4–6] and diagnostic [7–9] procedures, or improving food processing technologies [10]. Our interest in this topic has been motivated by the need to theoretically assess exposures to radiation from devices used for wireless communications and power transfer. Ubiquitous deployment of this class of devices may be composed of emerging metamaterial-inspired [11–14] technologies and circuits once these solutions reach maturity.

Realistic mathematical descriptions of the dielectric properties are mostly obtained by fitting the parameters of a theoretical model in accordance with the measured data points. The behavior of the relative complex permittivity ε of biological tissues with frequency is usually described with the help of empirical models such as the Debye [15] or Cole-Cole [16] functions, as described in [17–19].

It is well known that the physical properties of tissues are sensitive to temperature. A useful survey regarding the temperature dependent properties of tissues may be found in [20, 21]. In [22], the measured variation of the relative permittivity and conductivity of blood, at a given frequency, with temperature was modeled by the linear law. The results were obtained from evaluations on human and animal (cow, sheep) blood in the temperature range 25°C–45°C and the frequency range 1 MHz–1 GHz. The reference temperature, or T_r in our notation (see below), was taken as 25°C. The appertaining

Received 27 January 2021, Accepted 3 March 2021, Scheduled 9 March 2021

* Corresponding author: Mykola Zhuk (mykola.zhuk@canada.ca).

The authors are with the Consumer and Clinical Radiation Protection Bureau, Health Canada, 775 Brookfield Road, A. L. 6302C, Ottawa, Ontario K1A 1C1, Canada.

first-order temperature coefficients of relative permittivity and conductivity of blood as functions of frequency were presented in graphical form. The dielectric properties of human blood in the frequency range from 1 Hz to 40 GHz and the temperature range from about 7°C to $\sim$ 57°C, were experimentally studied in [23]. A combination of models for different dispersion regions was developed, including the temperature-dependent parameters of the first-order Cole-Cole function, with the fit parameters presented in graphical and table forms as functions of temperature. In [24], the bovine and porcine liver tissues were experimentally studied, where the wideband (0.5 GHz to 20 GHz) frequency dependence of their dielectric properties was described with the help of a first-order Cole-Cole model. The study concluded that the temperature dependence (from room temperature to $\sim$ 60°C) can be modeled by choosing the four Cole-Cole parameters as second-degree polynomials of temperature. In a recent paper [25], porcine liver, muscle, fat, and blood were experimentally characterized in the temperature range between 30°C and 50°C, in the microwave frequency range of 0.5 GHz to 27 GHz. To describe the frequency dependence of the measured data, a second-order Cole-Cole model with six free parameters was assumed, where the Cole-Cole parameters were taken as second-degree polynomials of temperature.

While the Cole-Cole function is a widespread model, from a practical point of view a more convenient approximation would consist of a version which has a simpler form. For example, it is quite useful to characterize the dielectric properties over a select range of temperatures with the help of temperature coefficients. This amounts to representing the dielectric functions as polynomials of the temperature variable (T). This form also considers the following aspects: *i*) a slow varying dielectric quantity with respect to T is described with a single linear temperature coefficient, *ii*) to address a strong temperature dependence, knowledge of the linear and quadratic temperature coefficients usually suffices, and *iii*) frequency dispersion is naturally incorporated into this framework by setting the polynomial or temperature coefficients as functions of frequency variable (f).

The goal of this paper is twofold: first, we develop an efficient procedure to approximate the parametric mathematical functions used to model the frequency and temperature dependence of dielectric properties, by using polynomials of T, whose coefficients are in turn polynomials of f. Hence, the algorithm enables us to express the temperature coefficients of the complex permittivity as rational functions of frequency. Second, we apply our algorithm to the Cole-Cole models of tissue properties developed in [24, 25] over wide frequency and temperature ranges, and convert them into simple polynomial models. For reference purposes, we present explicit polynomial approximations for the real $\varepsilon'(f,T)$ and imaginary $\varepsilon''(f,T)$ parts of the relative complex permittivity functions that match those from [24, 25] with a relative error of less than 1% (the error metrics is described below).

A common way to develop a polynomial approximation for a given function is to use a least squares fit. However, a least squares fit can allow large magnitude deviations from the basic formulation. Another obvious method is to use a partial sum of the power series for $\varepsilon'(f,T)$, $\varepsilon''(f,T)$ as functions of f,T (a variation of this method using a univariate power series of T is illustrated in Section 3). Unfortunately, the accuracy of all these methods is hard to control.

The principal idea of our approximation procedure is to represent the dielectric functions $\varepsilon'(f,T)$, $\varepsilon''(f,T)$ as expansions in the basis of bivariate Chebyshev polynomials of the first kind [26, Sec. 5.3.3], and then truncate the resulting bivariate Chebyshev series after a finite number of terms. The expansion coefficients of the bivariate Chebyshev series are easily calculated numerically via a midpoint quadrature rule.

The main reason that we chose to work with the Chebyshev polynomials (henceforth understood to refer exclusively to Chebyshev polynomials of the first kind) is that for a continuous function of several variables a truncated multivariate Chebyshev series produces a near-best polynomial approximation [27]. In practical terms, this means that for a dielectric function of f,T, the partial sum of a given order is virtually indistinguishable from the best polynomial approximation, which minimizes the maximal absolute deviation from the true function for bivariate polynomials of the same order. Owing to the fact that the Chebyshev polynomials are bounded between -1 and 1 in the region of interest, the truncation error can be (unrigorously) estimated as the maximal coefficient of the discarded terms. For well-behaved functions, including the aforementioned functions, the expansion coefficients tend rapidly to zero [27, 28].

The approximation procedure presented in this paper has two major limitations. One is that the polynomial representation of frequency dependence, unlike the Debye representation, can not

be efficiently incorporated into the finite-difference time-domain (FDTD) modeling of dispersive materials [29, Ch. 9] because the powers of the frequency give rise to the derivatives in the time domain. The other challenge concerns the approximation of functions over large measurement domains — as the size of a domain increases, a multivariate Chebyshev series approach may involve a large number of terms, thus rendering it impracticable.

The paper is organized as follows. A presentation of the Chebyshev series approximation method is found in Section 2. In Section 3, we briefly describe the concept of temperature coefficients and review (for comparison purposes) the power series approximation of the dielectric functions. In Section 4, the Chebyshev series method is applied to the benchmark temperature-dependent Cole-Cole models of biological tissues from [24] and [25], giving a very good illustration of the efficiency of our procedure. The numerical results have shown the unsuitability of the commonly used power-of-f representation of the polynomials concerned due to large rounding errors when the frequency range is large. We resolve this problem by expressing the appertaining coefficients as polynomials in the transformed frequency variable $x(f)$ in the Chebyshev basis. In Appendix A, we provide a simple scheme for determining the domain of convergence of the power series for the temperature-dependent Cole-Cole models by extending the latter into the complex T-domain. In the important case where the Cole-Cole parameters are the second-degree polynomials in the temperature variable, the radius of convergence can be found analytically.

In the following, the constants $F_{\min}$, $F_{\max}$ ($F_{\max} > F_{\min}$) and $T_{\min}$, $T_{\max}$ ($T_{\max} > T_{\min}$) denote the end points of the intervals in the frequency and temperature domains, from which the approximations for ε', ε'' will be developed. When we specifically deal with the permittivity functions from [24, 25], these constants have the meaning of the end points of the measurement intervals employed in both cited papers. Namely, when we refer to the results of [24], it is assumed that:

$$F_{\min} = 0.5\,\text{GHz}, \quad F_{\max} = 20\,\text{GHz}, \tag{1.1}$$

$$T_{\min} = 23^{\circ}\text{C}, \quad T_{\max} = 60^{\circ}\text{C} \tag{1.2}$$

(note that the lower temperature bound is not specified precisely in [24], and we interpret it from the plots therein). Additionally, whenever we make use of the model of [25], the aforementioned constants are understood to have the following values:

$$F_{\min} = 0.5\,\text{GHz}, \quad F_{\max} = 7\,\text{GHz}, \tag{1.3}$$

$$T_{\min} = 30^{\circ}\text{C}, \quad T_{\max} = 50^{\circ}\text{C}. \tag{1.4}$$

We shall assume, except where otherwise specified, that:

$$F_{\min} \le f \le F_{\max}, \tag{1.5}$$

$$T_{\min} \le T \le T_{\max}. \tag{1.6}$$

Also, we have further use for the lengths of the approximation/measurement intervals

$$\Delta F = F_{\max} - F_{\min}, \tag{1.7}$$

$$\Delta T = T_{\max} - T_{\min} \tag{1.8}$$

and the midpoint of the temperature range

$$T_m = \frac{1}{2}(T_{\max} + T_{\min}). \tag{1.9}$$

For notational simplicity, the quantities ε', ε'' will be collectively referred to as ν. When we use the results of [24] or [25] for a numerical illustration, the quality of an approximation $\nu_{\text{approx}}(f, T)$ to the true function $\nu_{\text{true}}(f, T)$ will be quantified by the relative error $r, \%$,

$$r = 100 \max_{p,q} \left| \frac{\nu_{\text{true}}(f_p, T_q) - \nu_{\text{approx}}(f_p, T_q)}{\nu_{\text{true}}(f_p, T_q)} \right| \tag{1.10}$$

calculated by sweeping over discrete frequencies f_p in 10 MHz steps and discrete temperatures T_q with 0.2°C steps (the systems $\{f_p\}$, $\{T_q\}$ include the end points of the intervals in Eqs. (1.5), (1.6). Note that we shall use the same frequency and temperature spacings for both the measurement intervals in Eqs. (1.1), (1.2) and in Eqs. (1.3), (1.4). The relative error $r, \%$ is evaluated for the approximating expressions exactly as they are written below. When reporting a numerical value of the relative error, the original result calculated according to Eq. (1.10) is always rounded up.

We used Wolfram Mathematica 12 from Wolfram Research (Champaign, IL) to complete this work.

2. THE CHEBYSHEV SERIES METHOD

The chief tool that we use in this section is the double series expansion of a function that uses the form: $\{\mathfrak{T}_m(x)\mathfrak{T}_n(y)\}_{m,n=0}^{\infty}$, which is composed of products of two univariate Chebyshev polynomials $\mathfrak{T}_m(x)$, $\mathfrak{T}_n(y)$. The Chebyshev polynomial $\mathfrak{T}_m(x)$ of degree m at the point x is defined by the following recurrence relation [26, Eqs. (1.3a), (1.3b)]

$$\mathfrak{T}_0(x) = 1, \tag{2.1}$$
$$\mathfrak{T}_1(x) = x, \tag{2.2}$$
$$\mathfrak{T}_m(x) = 2x\mathfrak{T}_{m-1}(x) - \mathfrak{T}_{m-2}(x), \quad (m = 2, 3, \ldots) \tag{2.3}$$

Below, $\mathfrak{T}_n(y)$ will denote the same function of n, y as $\mathfrak{T}_m(x)$ is of m, x.

Let $x(f)$ and $y(T)$ be the normalized frequency and temperature variables defined by

$$x(f) = \frac{1}{\Delta F}(2f - F_{\min} - F_{\max}), \tag{2.4}$$
$$y(T) = \frac{1}{\Delta T}(2T - T_{\min} - T_{\max}) \tag{2.5}$$

It is easy to verify that

$$x(F_{\min}) = -1, \quad x(F_{\max}) = 1, \tag{2.6}$$
$$y(T_{\min}) = -1, \quad y(T_{\max}) = 1. \tag{2.7}$$

Note that the aforementioned functions are invertible at every point of their domains, and their respective inverse functions are:

$$f(x) = \frac{1}{2}(x\Delta F + F_{\min} + F_{\max}), \tag{2.8}$$
$$T(y) = \frac{1}{2}(y\Delta T + T_{\min} + T_{\max}). \tag{2.9}$$

The reason for introducing the functions $f(x), T(y)$ is that the generic dielectric function $\nu(f, T)$ can be regarded as a function of x, y on the unit square

$$D = \{x, y : -1 \le x \le 1, -1 \le y \le 1\}. \tag{2.10}$$

On the assumption that $\nu(f(x), T(y))$ is continuous on D, it can be characterized by the following bivariate Chebyshev series [26, Sec. 5.3.3]:

$$C(x(f), y(T))) = \sum_{m,n=0}^{+\infty} c_{mn}\mathfrak{T}_m(x(f))\mathfrak{T}_n(y(T)), \tag{2.11}$$

where the coefficients c_{mn} are defined as

$$c_{mn} = \frac{1}{S_m S_n}\int_{-1}^{1}\int_{-1}^{1}\nu(f(x), T(y))\frac{\mathfrak{T}_m(x)\mathfrak{T}_n(y)}{\sqrt{1-x^2}\sqrt{1-y^2}}\,dxdy \quad (m, n = 0, 1, 2, \ldots) \tag{2.12}$$

with

$$S_m = \frac{\pi}{2}\begin{cases} 2 & (m = 0) \\ 1 & (m \ne 0) \end{cases} \tag{2.13}$$

The series $C(x, y)$ converges to $\nu(f(x), T(y))$ uniformly on D if the latter function satisfies some additional conditions beyond continuity on D [26, Thm. 5.9, Sec. 5.3.3]. We will not address fine mathematical points related to the convergence, and instead emphasize a principal merit that makes the Chebyshev series (2.11) notable: its partial sum of order $m_{\max}, n_{\max}$ in x, y, respectively, forms a near-best approximation to the continuous function $\nu(f(x), T(y))$ [27]. Simply put, it is very nearly the same polynomial as the minimax polynomial of order $m_{\max}, n_{\max}$ which, among the bivariate polynomials of x, y of the same order, has the smallest maximum deviation on D from the target function $\nu(f(x), T(y))$.

Another nice property of the Chebyshev series in Eq. (2.11) which follows from a relevant property of the univariate Chebyshev polynomials (cf Eq. (1.1) from [26, Sec. 1.2.1]) is that $|\mathfrak{T}_m(x)\mathfrak{T}_n(y)| \leq 1$ on D. Assuming (unrigorously) that the absolute error due to truncation of a series is of the same order as the maximal discarded *term*, we then obtain a convenient estimate of the truncation error as the maximal discarded *coefficient*. If $\nu(f(x), T(y))$ satisfies certain analyticity assumptions, the coefficients c_{mn} decrease geometrically with the indices m, n [28, Lem. 5.1].

In view of the preceding, the development of a practical approximation to $\nu(f, T)$ can be done in the following way: a) truncate the Chebyshev series in Eq. (2.11) at the (sufficiently large) indices $m_{\max}, n_{\max}$ assuming that c_{mn} are negligible beyond the index set $m_{\max}, n_{\max}$, b) compute the coefficients $c_{m,n}$ for $m = 0, 1, \ldots, m_{\max}$, $n = 0, 1, \ldots, n_{\max}$, c) define an approximate cut-off bound δ ($\delta > 0$), and replace by zeros the computed coefficients such that $|c_{mn}| < \delta$, d) (optionally) cull the retained coefficients c_{mn} further in order to reduce the degree L of the resulting polynomial in Eq. (2.14) in the temperature variable, and e) express $\mathfrak{T}_n(y(T))$ in terms of powers of T. These steps produce an approximate formula for $\nu(f, T)$ in the form

$$\nu(f, T) \approx b_0 + b_1 T + b_2 T^2 + \ldots + b_L T^L, \tag{2.14}$$

where the coefficients $b_0, b_1, \ldots, b_L$ are polynomials in f which are naturally expressible in terms of the Chebyshev polynomials $\mathfrak{T}_m(x(f))$. The latter can be expanded in terms of powers of f; however, this is not recommended because we may lose in the accuracy of computations — see Section 4.

To implement the aforementioned procedures in a practical sense, we need a method for evaluating the Chebyshev coefficients c_{mn} from Eq. (2.12). Writing $x = \cos\theta_x$, $y = \cos\theta_y$, the coefficient c_{mn} will be:

$$c_{mn} = \frac{1}{S_m S_n} \int_0^\pi \int_0^\pi \nu(f(\cos\theta_x), T(\cos\theta_y)) \cos(m\theta_x) \cos(n\theta_y)\, d\theta_x d\theta_y, \tag{2.15}$$

where we have used the equalities $T_m(\cos\theta_x) = \cos m\theta_x$, $T_n(\cos\theta_y) = \cos n\theta_y$ [26, Eq. (1.1)]. (Obviously, the subscripts in θ_x, θ_y do not stand for differentiation with respect to x, y.)

An efficient way to compute the integrals in the right-hand side of Eq. (2.15) is the use of the rectangle (midpoint) quadrature rule. With this method in mind, let us partition the interval $0 < \theta_x < \pi$ into $M + 1$ subintervals

$$[(k-1)\Delta\theta_x, k\Delta\theta_x], \quad (k = 1, 2, \ldots, M+1) \tag{2.16}$$

of the same length

$$\Delta\theta_x = \frac{\pi}{M+1} \tag{2.17}$$

and the midpoints

$$\theta_{xk} = \frac{\pi(k - 1/2)}{M+1}. \tag{2.18}$$

Similarly, we break up the interval $0 < \theta_y < \pi$ into $N + 1$ subintervals

$$[(l-1)\Delta\theta_y, l\Delta\theta_y], \quad (l = 1, 2, \ldots, N+1) \tag{2.19}$$

with the length

$$\Delta\theta_y = \frac{\pi}{N+1} \tag{2.20}$$

and the midpoints

$$\theta_{yl} = \frac{\pi(l - 1/2)}{N+1}. \tag{2.21}$$

Then a numerical approximation to the integral in Eq. (2.15) is given by

$$c_{mn} \approx \frac{\Delta\theta_x}{S_m} \frac{\Delta\theta_y}{S_n} \sum_{k=1}^{M+1} \sum_{l=1}^{N+1} \nu(f(\cos\theta_{xk}), T(\cos\theta_{yl})) \cos(m\theta_{xk}) \cos(n\theta_{yl}). \tag{2.22}$$

— cf. [26, Eq. (5.38)]. Our own experience in using this quadrature formula suggests that a satisfactory accuracy is achieved if one chooses $M = 10m_{\max}$, $N = 10n_{\max}$. Such choice of parameters M, N is assumed in the numerical examples to follow.

3. TEMPERATURE COEFFICIENTS

The key concept of temperature coefficients is motivated by the following (approximate or exact) description of the dielectric property $\nu(f,T)$ as a function of temperature:

$$\nu(f,T) \approx \xi \left[1 + \sum_{k=1}^{L} \Lambda_k (T - T_r)^k\right]. \tag{3.1}$$

Here T_r is some reference temperature (which is usually set to the midpoint temperature T_m); the constant ξ is the estimate of $\nu(f,T)$ at the reference temperature; and Λ_k is the k-th order temperature coefficient. Note that the reference temperature T_r and the degree L may be different for $\nu = \varepsilon'$ and $\nu = \varepsilon''$. The temperature coefficients and the constant ξ in general may depend upon f and T_r: $\Lambda_k = \Lambda_k(f,T_r)$, $\xi = \xi(f,T_r)$.

If we expand the right-hand side of Eq. (2.14) in powers of $T - T_r$, where T_r is an arbitrary reference temperature, the result can obviously made into a form Eq. (3.1) with

$$\xi(f,T_r) = \sum_{l=0}^{L} b_l T_r^l, \tag{3.2}$$

$$\Lambda_k(f,T_r) = \frac{1}{\xi(f,T_r)} \sum_{l=k}^{L} \binom{l}{k} b_l T_r^{l-k}, \quad (k = 1,2,\ldots,L), \tag{3.3}$$

$$\binom{l}{k} = \frac{l!}{k!(l-k)!}. \tag{3.4}$$

These equations define a family of frequency-dependent temperature coefficients $\Lambda_k(f,T_r)$ as rational functions of f. Note that although our quantities $\xi(f,T_r)$, $\Lambda_k(f,T_r)$ are specific to a particular value of T_r, when used in the right-hand side of Eq. (3.1), they yield an expression (2.14) that does not depend upon T_r. In other words, the accuracy of the approximate expression (3.1) does not depend upon the reference temperature if the quantities $\xi(f,T_r)$, $\Lambda_k(f,T_r)$ are calculated within the Chebyshev series approach.

Another way to arrive at an approximation of the form of Eq. (3.1) is to develop $\nu(f,T)$ as a power series in $T - T_r$. This method works for those $\nu(f,T)$ that are real analytic functions of T at $T = T_r$. Within the frames of such an approach, the temperature coefficients are calculated as follows

$$\Lambda_k(f,T_r) = \frac{1}{k!\nu(f,T_r)} \frac{\partial^k \nu(f,T)}{\partial T^k}\bigg|_{T=T_r}, \tag{3.5}$$

and the constant ξ is determined by

$$\xi(f,T_r) = \nu(f,T_r). \tag{3.6}$$

The aforementioned approach requires that the power series concerned converge for each frequency and temperature from Eqs. (1.5), (1.6), hence the domain of convergence of the power series needs to be ascertained. For this, we will treat $\nu(f,T)$ as an analytic function in the complex T-plane (see Appendix A). Table A1 of Appendix A reveals that, for $T_r = T_m$, the power series of the experimental Cole-Cole functions from [24, 25] have the radius of convergence that does not depend upon frequency and well exceeds the halfwidth $\frac{1}{2}\Delta T$ of the temperature range. However, we are unable to give a realistic estimate of the rate of convergence of those power series, or to estimate the improvement, if any, of the approximation with the degree L. Note that the analytic differentiation in Eq. (3.5), while elementary, may be tedious, and the resulting expressions are extremely cumbersome when the exact dielectric functions are described by the Debye [15] or Cole-Cole [16] models with the temperature-dependent parameters.

For lack of better information, we illustrate in Table 1 the rationality of the Chebyshev series approximations listed in Section 4 and of the power series approximations of the same degree L by calculating the relative error of these approximations to the measured dielectric functions of several tissues from [24] and [25]. According to these results, we gain better accuracy by using the Chebyshev series approach.

Table 1. Relative error $r, \%$, of approximation (3.1) to the experimental dielectric functions, for the Chebyshev series method (3.2)–(3.3) and the power series method (3.5)–(3.6) with $T_r = T_m$.

Method	Liver [24]		Liver [25]		Muscle [25]		Fat [25]		Blood [25]	
	ε'	ε''	ε'	ε''	ε'	ε''	ε'	ε''	ε'	ε''
Cheb.	0.19	0.46	0.25	0.73	0.18	0.86	0.60	0.11	0.40	0.20
Power	1.12	3.59	0.40	1.41	0.33	1.71	1.15	0.37	0.80	0.60

From an application point of view, it is highly desirable to characterize a dielectric function $\nu(f, T)$ with less temperature coefficients, ie to use a polynomial in T of the lowest degree L while preserving the desired accuracy. As can be seen from Table 2, this is better realized in the Chebyshev series approximation. With reference to the experimental results of [25], only one temperature coefficient is necessary to describe the porcine liver or muscle ε', ε'' and the porcine fat or blood ε', and two temperature coefficients — for the porcine fat or blood ε''. The ultra-wideband dielectric properties of animal liver [24] can be described with three temperature coefficients for each of the quantities ε', ε''.

Table 2. Degree L of approximation (3.1) in the temperature variable T that provides a relative error of $r \leq 1\%$ to the experimental dielectric functions, for the Chebyshev series method (3.2)–(3.3) and the power series method (3.5)–(3.6) with $T_r = T_m$.

Method	Liver [24]		Liver [25]		Muscle [25]		Fat [25]		Blood [25]	
	ε'	ε''	ε'	ε''	ε'	ε''	ε'	ε''	ε'	ε''
Cheb.	3	3	1	1	1	1	1	2	1	2
Power	4	5	1	2	1	2	2	2	1	2

Plots for the selected temperature coefficients as functions of frequency are shown in the next section. In these plots, the temperature coefficients of the real and imaginary parts ε', ε'' of the complex permittivity are marked by primes and double primes as Λ_k' and Λ_k'', accordingly. Specifically, Figs. 2, 4, 6 and 8 give the temperature coefficients for porcine liver, muscle, fat and blood, respectively, based on the experimental results from [25], and Fig. 10 — for the animal liver results from [24]. These plots demonstrate that the numerical values of the temperature coefficients based on Eq. (3.3) and on the power series approximation in Eq. (3.5) with $T_r = T_m$ are quite close.

4. PRACTICAL DIELECTRIC FUNCTIONS

Our aim here is to provide the Chebyshev series approximations to several wideband temperature-dependent Cole-Cole models of biological tissues. The sources of the experimental dielectric functions are [24] and [25].

Tables 3 and 4 illustrate the rapid improvement of the approximations that we have developed with the degree L of approximation in the temperature variable.

Table 3. Relative error $r, \%$, of the Chebyshev series approximation (2.14) to the measured dielectric functions from [24] vs degree L in the temperature variable T.

L	1	2	3	4
ε'	1.47	1.18	0.19	0.062
ε''	4.45	1.82	0.46	0.29

Table 4. Relative error $r, \%$, of the Chebyshev series approximation (2.14) to the measured dielectric functions from [25] vs degree L in the temperature variable T.

L	Liver		Muscle		Fat		Blood	
	ε'	ε''	ε'	ε''	ε'	ε''	ε'	ε''
1	0.27	0.73	0.18	0.86	0.60	1.59	0.40	1.34
2	0.087	0.14	0.077	0.13	0.088	0.11	0.078	0.20
3	n/a	0.093	n/a	0.079	n/a	0.082	n/a	0.094

Our special interest has been in evaluating the effect of the representation of the numerical coefficients on the accuracy of the approximations concerned. On this subject, we note that the frequency-dependent coefficients $b_0, b_1, \ldots, b_L$ from Eq. (2.14) can be given in two forms, namely as functions of the transformed variable $x(f)$ (2.4), and as polynomials of the frequency variable f — e.g., Eqs. (4.1), (4.2) and Eqs. (4.3), (4.4). Under finite-precision arithmetic, however, the familiar "power-of-f" form may be the cause of a large rounding error. How this comes about is illustrated in Table 5. This table refers to the imaginary part of complex permittivity of porcine muscle from [25], and gives the relative error $r, \%$ of the quadratic ($L = 2$) Chebyshev series approximation (2.14) for ε'' in the case where the coefficients b_0 and b_1 from Eqs. (4.11), (4.12) are expressed in the "power-of-f" basis. The parameter N_s is the number of significant digits kept in the *fractional* part of the numerical coefficients of the powers of f. Two things stand out very markedly about these results. First, as compared to the x-domain representation in the Chebyshev basis, extra significant digits ($N_s = 11 \ldots 12$) are needed to keep the relative error at an acceptable level. Second, writing b_0, b_1 in the power form with the insufficient precision in the coefficients may be the cause of catastrophic rounding errors. We here resolve this problem by expressing the coefficients $b_0, b_1, \ldots, b_L$ in the Chebyshev basis in the x domain (the other technique being the extended-precision calculations).

Table 5. Relative error $r, \%$, of the quadratic approximation (2.14), (4.11), (4.12) to the measured ε'' of porcine muscle [25] vs N_s in the "power-of-f" expansion for the coefficients b_0, b_1.

N_s	7	8	9	10	11	12
$r, \%$	555	91	1.78	0.71	0.13	0.13

The graphical representations of the approximations for the dielectric functions that we have discussed are given in Figs. 1, 3, 5, and 7 for porcine liver, muscle, fat and blood, respectively, based on the experimental results from [25], and in Fig. 9 — for the animal liver results from [24]. As can be seen from these figures, the agreement between the approximate formulations and the original experimental data is exceedingly good.

4.1. Porcine Liver [25, Table 1]

ε': $L = 1$, $r = 0.25\%$,

$$\begin{aligned} b_0 \;=\; & 46.6678 - 7.5879\mathfrak{T}_1(x) + 0.4524\mathfrak{T}_2(x) - 0.1292\mathfrak{T}_3(x) \\ & +0.08942\mathfrak{T}_4(x) - 0.05316\mathfrak{T}_5(x) + 0.02998\mathfrak{T}_6(x) \\ & -0.05396\mathfrak{T}_7(x) + 0.03048\mathfrak{T}_8(x) - 0.01727\mathfrak{T}_9(x), \end{aligned} \tag{4.1}$$

$$\begin{aligned} b_1 \;=\; & -0.04607 + 0.05276\mathfrak{T}_1(x) + 0.0147\mathfrak{T}_2(x) - 0.01029\mathfrak{T}_3(x) \\ & +0.005399\mathfrak{T}_4(x) - 0.002945\mathfrak{T}_5(x) + 0.001647\mathfrak{T}_6(x). \end{aligned} \tag{4.2}$$

In the frequency domain:

$$\begin{aligned} b_0 \;=\; & 61.4064124 - 22.3523746f + 28.349677f^2 - 22.1333128f^3 \\ & +10.3497087f^4 - 3.02332181f^5 + 0.5571493f^6 \\ & -0.06302658f^7 + 0.004001336f^8 - 0.0001092707f^9, \end{aligned} \tag{4.3}$$

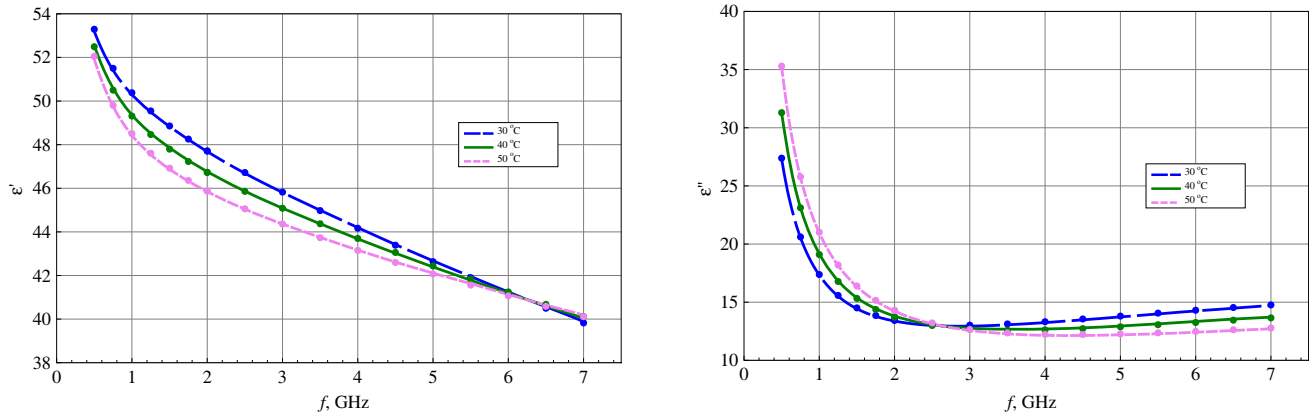

Figure 1. Dielectric properties ε', ε'' of porcine liver at three different temperatures based on the approximations from Section 4.1 (solid lines), and the results reported in [25, Sec. 4.1] (dots).

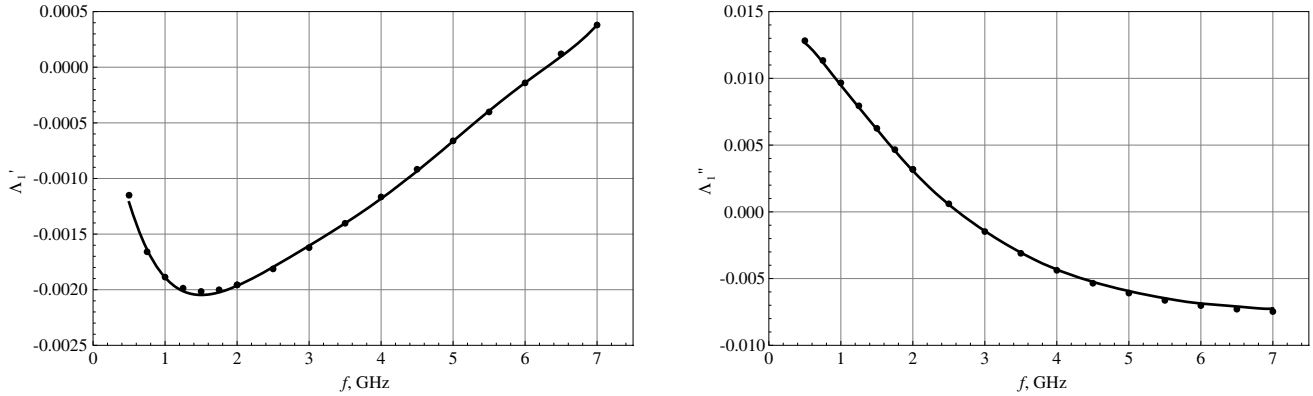

Figure 2. Temperature coefficients of the complex dielectric permittivity of porcine liver based on Eq. (3.3) and the approximations from Section 4.1 (solid lines), and on the power series approximation (3.5) (dots), for $T_r = T_m$.

$$b_1 = 0.01450895 - 0.2279394f + 0.1697456f^2 - 0.06009775f^3 + 0.01154731f^4 - 0.001136054f^5 + 0.00004471628f^6. \quad (4.4)$$

ε'': $L = 1$, $r = 0.73\%$,

$$b_0 = 14.864 + 2.6523\mathfrak{T}_1(x) + 0.7684\mathfrak{T}_2(x) - 0.9707\mathfrak{T}_3(x) + 0.6215\mathfrak{T}_4(x) - 0.3648\mathfrak{T}_5(x) + 0.2110\mathfrak{T}_6(x) - 0.1216\mathfrak{T}_7(x) + 0.07001\mathfrak{T}_8(x) - 0.04028\mathfrak{T}_9(x) + 0.02317\mathfrak{T}_{10}(x) - 0.03034\mathfrak{T}_{11}(x) + 0.01739\mathfrak{T}_{12}(x) - 0.009975\mathfrak{T}_{13}(x) + 0.005724\mathfrak{T}_{14}(x), \quad (4.5)$$

$$b_1 = 0.02531 - 0.1869\mathfrak{T}_1(x) + 0.08994\mathfrak{T}_2(x) - 0.04277\mathfrak{T}_3(x) + 0.02289\mathfrak{T}_4(x) - 0.01274\mathfrak{T}_5(x) + 0.007165\mathfrak{T}_6(x) - 0.004052\mathfrak{T}_7(x) + 0.002299\mathfrak{T}_8(x) - 0.001308\mathfrak{T}_9(x) + 0.0007452\mathfrak{T}_{10}(x). \quad (4.6)$$

In the frequency domain:

$$b_0 = 60.1621161272 - 243.0116514447f + 579.2961160339f^2 - 842.320228251f^3 + 815.4104970348f^4 - 550.7609349484f^5 + 267.4197891336f^6 - 95.02694983356f^7 + 24.9098280334f^8 - 4.8083534666f^9 + 0.6746957636f^{10}, \quad (4.7)$$

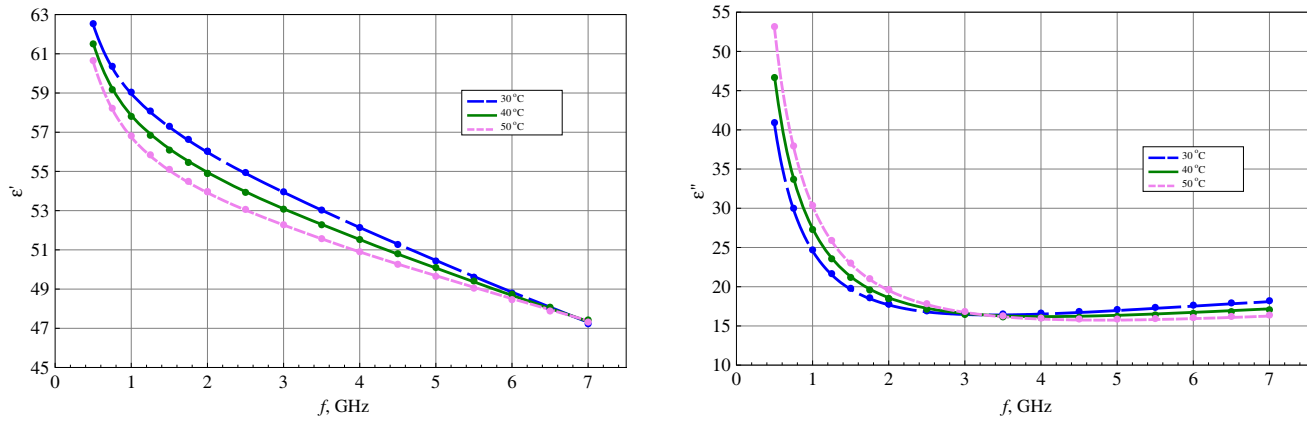

Figure 3. Dielectric properties ε', ε'' of porcine muscle at three different temperatures based on the approximations from Section 4.2 (solid lines), and the results reported in [25, Sec. 4.2] (dots).

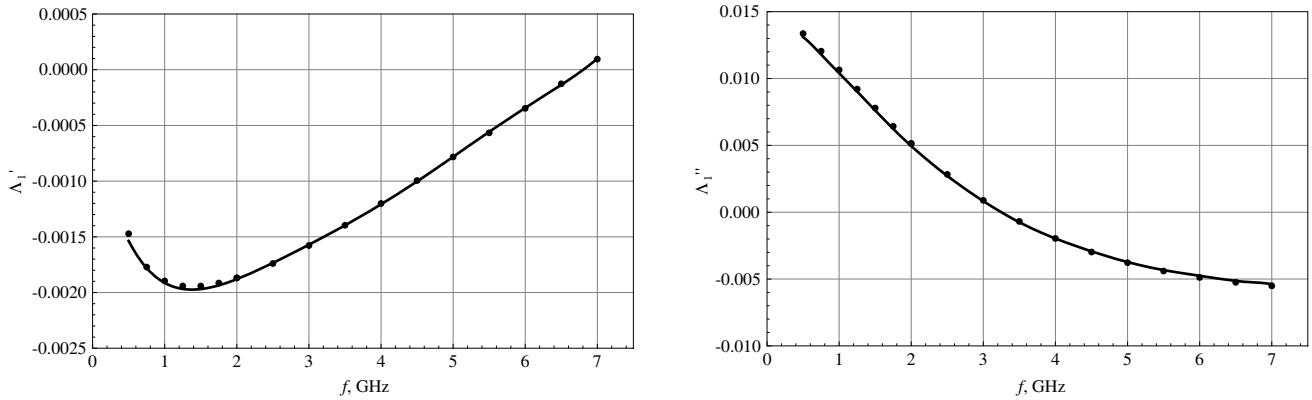

Figure 4. Temperature coefficients for the complex dielectric permittivity of porcine muscle based on Eq. (3.3) and the approximations from Section 4.2 (solid lines), and on the power series approximation (3.5) (dots), for $T_r = T_m$.

$$\begin{aligned} b_1 \;=\; & 1.1695318708 - 2.7978340348 f + 3.6690071226 f^2 - 3.006511116316 f^3 \\ & + 1.5970250289 f^4 - 0.5639051466 f^5 + 0.1333297839 f^6 - 0.02083564929 f^7 \\ & + 0.002062799972 f^8 - 0.0001171049527 f^9 + 10^{-6} \cdot 2.90212257 f^{10}. \end{aligned} \tag{4.8}$$

The dimension of the cyclic frequency f, as it appears in Eqs. (4.3), (4.4), (4.7), (4.8), is the gigahertz.

4.2. Porcine Muscle [25, Table 2]

ε': $L = 1$, $r = 0.18\%$,

$$\begin{aligned} b_0 \;=\; & 55.1698 - 8.5142\mathfrak{T}_1(x) + 0.7330\mathfrak{T}_2(x) - 0.3500\mathfrak{T}_3(x) + 0.2198\mathfrak{T}_4(x) - 0.1265\mathfrak{T}_5(x) \\ & + 0.07140\mathfrak{T}_6(x) - 0.06441\mathfrak{T}_7(x) + 0.03650\mathfrak{T}_8(x) - 0.02074\mathfrak{T}_9(x) + 0.01181\mathfrak{T}_{10}(x), \end{aligned} \tag{4.9}$$

$$\begin{aligned} b_1 \;=\; & -0.05984 + 0.05851\mathfrak{T}_1(x) + 0.01032\mathfrak{T}_2(x) - 0.006992\mathfrak{T}_3(x) \\ & + 0.003502\mathfrak{T}_4(x) - 0.001898\mathfrak{T}_5(x) + 0.001065\mathfrak{T}_6(x). \end{aligned} \tag{4.10}$$

ε'': $L = 1$, $r = 0.86\%$,

$$\begin{aligned} b_0 \;=\; & 18.2753 + 1.6918\mathfrak{T}_1(x) + 1.8778\mathfrak{T}_2(x) - 1.5891\mathfrak{T}_3(x) + 0.9506\mathfrak{T}_4(x) - 0.5443\mathfrak{T}_5(x) \\ & + 0.3103\mathfrak{T}_6(x) - 0.1769\mathfrak{T}_7(x) + 0.1009\mathfrak{T}_8(x) - 0.05763\mathfrak{T}_9(x) + 0.03294\mathfrak{T}_{10}(x) - 0.01884\mathfrak{T}_{11}(x) \\ & + 0.02804\mathfrak{T}_{12}(x) - 0.01612\mathfrak{T}_{13}(x) + 0.009266\mathfrak{T}_{14}(x) - 0.005329\mathfrak{T}_{15}(x), \end{aligned} \tag{4.11}$$

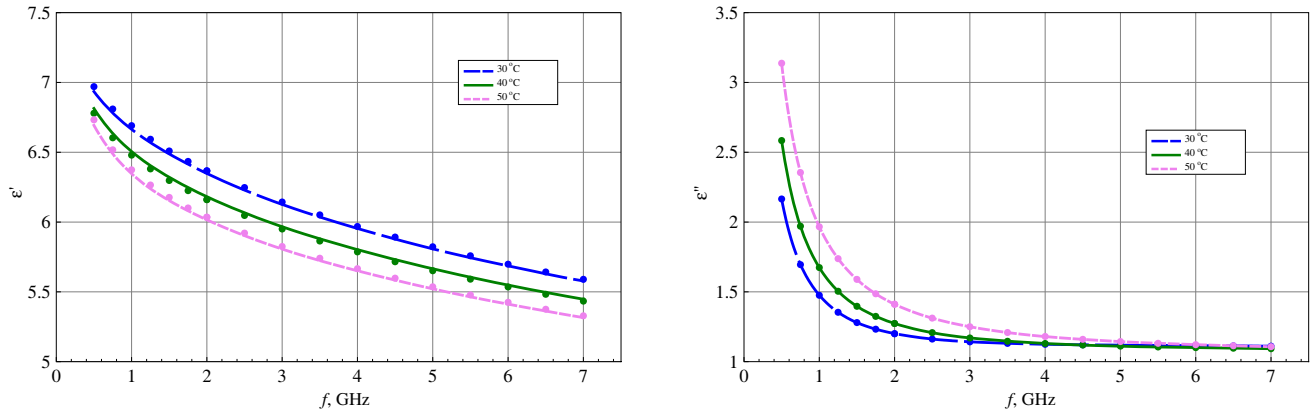

Figure 5. Dielectric properties of porcine fat at three different temperatures based on the approximations from Section 4.3 (solid lines), and the results reported in [25, Sec. 4.3] (dots).

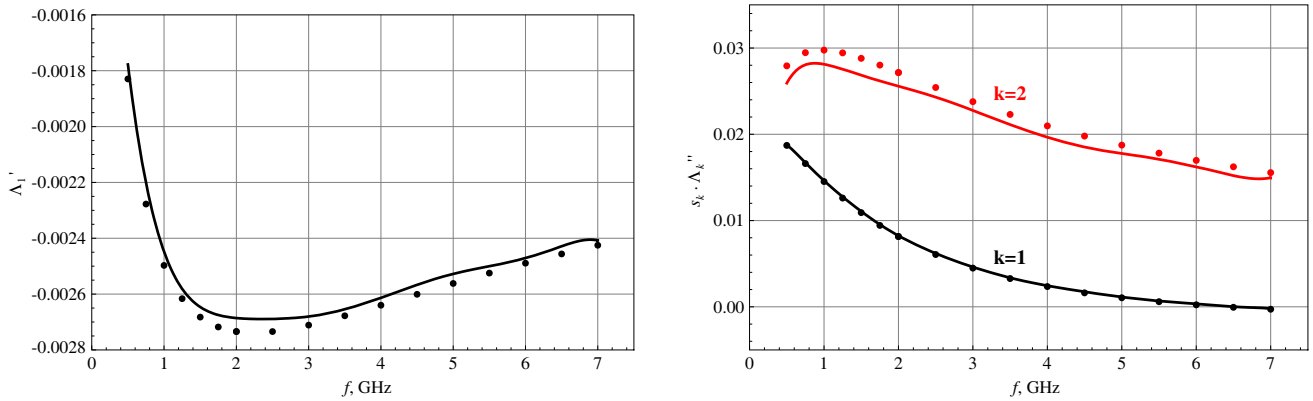

Figure 6. Temperature coefficients for the complex dielectric permittivity of porcine fat based on Eq. (3.3) and the approximations from Section 4.3, and on the power series approximation (3.5) (dots), for $T_r = T_m$. The scaling coefficient s_k is 1 for $k = 1$, and 10^2 for $k = 2$.

$$\begin{aligned} b_1 \;=\; & 0.07818 - 0.2562\mathfrak{T}_1(x) + 0.1284\mathfrak{T}_2(x) - 0.06599\mathfrak{T}_3(x) + 0.03682\mathfrak{T}_4(x) \\ & -0.02096\mathfrak{T}_5(x) + 0.01199\mathfrak{T}_6(x) - 0.00687\mathfrak{T}_7(x) + 0.003943\mathfrak{T}_8(x) \\ & -0.002266\mathfrak{T}_9(x) + 0.001303\mathfrak{T}_{10}(x) - 0.0007496\mathfrak{T}_{11}(x). \end{aligned} \tag{4.12}$$

4.3. Porcine Fat [25, Table 3]

ε': $L = 1$, $r = 0.60\%$,

$$\begin{aligned} b_0 \;=\; & 6.54496 - 0.65536\mathfrak{T}_1(x) + 0.091035\mathfrak{T}_2(x) - 0.011027\mathfrak{T}_3(x) - 0.00095369\mathfrak{T}_4(x) \\ & +0.0021116\mathfrak{T}_5(x) - 0.0016077\mathfrak{T}_6(x) + 0.0010348\mathfrak{T}_7(x) + 0.0017096\mathfrak{T}_8(x), \end{aligned} \tag{4.13}$$

$$\begin{aligned} b_1 \;=\; & -0.014599 + 0.00092458\mathfrak{T}_1(x) + 0.0012014\mathfrak{T}_2(x) - 0.00098439\mathfrak{T}_3(x) \\ & +0.00059538\mathfrak{T}_4(x) - 0.00033751\mathfrak{T}_5(x) + 0.00018837\mathfrak{T}_6(x) - 0.00010486\mathfrak{T}_7(x). \end{aligned} \tag{4.14}$$

ε'': $L = 2$, $r = 0.11\%$,

$$\begin{aligned} b_0 \;=\; & 1.4152 - 0.08743\mathfrak{T}_1(x) + 0.06564\mathfrak{T}_2(x) - 0.0581\mathfrak{T}_3(x) + 0.0398\mathfrak{T}_4(x) - 0.02468\mathfrak{T}_5(x) \\ & +0.01469\mathfrak{T}_6(x) - 0.003155\mathfrak{T}_7(x) + 0.002002\mathfrak{T}_8(x) - 0.001235\mathfrak{T}_9(x) + 0.0007497\mathfrak{T}_{10}(x) \\ & -0.00045\mathfrak{T}_{11}(x) + 0.001417\mathfrak{T}_{12}(x) - 0.0008166\mathfrak{T}_{13}(x) + 0.0004707\mathfrak{T}_{14}(x), \end{aligned} \tag{4.15}$$

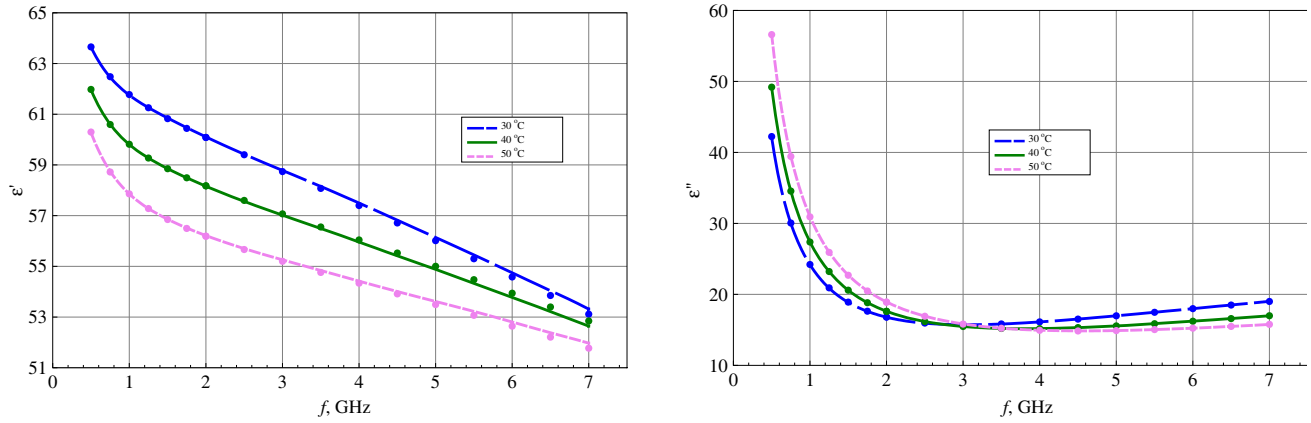

Figure 7. Dielectric properties of porcine blood at three different temperatures based on the approximations from Section 4.4 (solid lines), and the results reported in [25, Sec. 4.4] (dots).

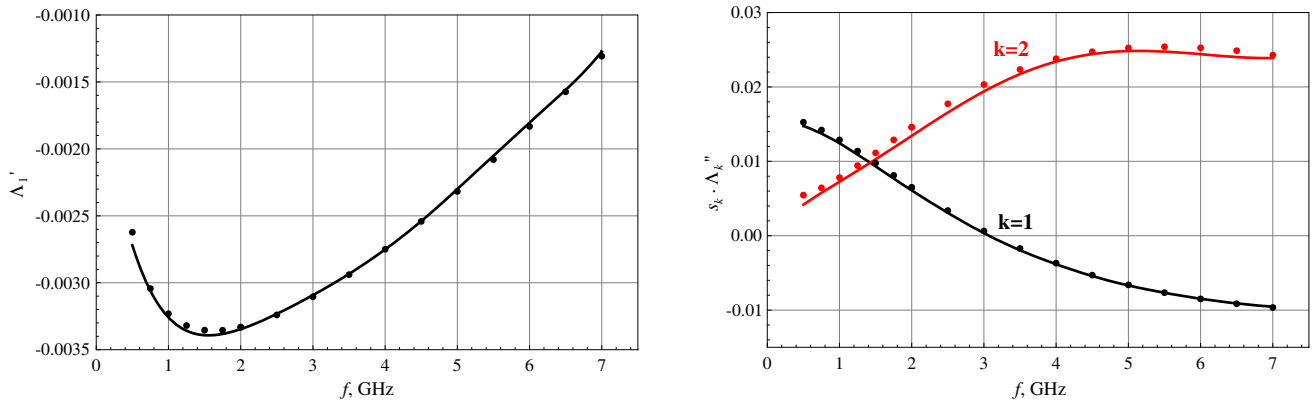

Figure 8. Temperature coefficients for the complex dielectric permittivity of porcine blood based on Eq. (3.3) and the approximations from Section 4.4 (solid lines), and on the power series approximation (3.5) (dots), for $T_r = T_m$. The scaling coefficient s_k is 1 for $k = 1$, and 10^2 for $k = 2$.

$$\begin{aligned} b_1 &= -0.01346 - 0.001211\mathfrak{T}_1(x) + 0.002599\mathfrak{T}_2(x) - 0.001646\mathfrak{T}_3(x) + 0.0009624\mathfrak{T}_4(x) \\ &\quad -0.0005654\mathfrak{T}_5(x) + 0.000335\mathfrak{T}_6(x) - 0.0004792\mathfrak{T}_7(x) + 0.0002715\mathfrak{T}_8(x) \\ &\quad -0.0001544\mathfrak{T}_9(x) + 0.00008797\mathfrak{T}_{10}(x) - 0.00005023\mathfrak{T}_{11}(x), \qquad (4.16) \\ b_2 &= 0.0003018 - 0.0001988\mathfrak{T}_1(x) + 0.00008622\mathfrak{T}_2(x) - 0.00004257\mathfrak{T}_3(x) \\ &\quad +0.00002227\mathfrak{T}_4(x) - 0.00001191\mathfrak{T}_5(x) + 10^{-6} \cdot 6.436\mathfrak{T}_6(x). \qquad (4.17) \end{aligned}$$

4.4. Porcine Blood [25, Table 4]

ε': $L = 1$, $r = 0.40\%$,

$$\begin{aligned} b_0 &= 62.2524 - 6.6012\mathfrak{T}_1(x) - 0.3233\mathfrak{T}_2(x) - 0.005475\mathfrak{T}_3(x) \\ &\quad +0.04398\mathfrak{T}_4(x) - 0.02699\mathfrak{T}_5(x) + 0.0152\mathfrak{T}_6(x) \\ &\quad -0.04156\mathfrak{T}_7(x) + 0.0239\mathfrak{T}_8(x) - 0.01376\mathfrak{T}_9(x), \qquad (4.18) \\ b_1 &= -0.1433 + 0.06214\mathfrak{T}_1(x) + 0.01969\mathfrak{T}_2(x) - 0.008936\mathfrak{T}_3(x) \\ &\quad +0.004395\mathfrak{T}_4(x) - 0.002481\mathfrak{T}_5(x) + 0.001429\mathfrak{T}_6(x). \qquad (4.19) \end{aligned}$$

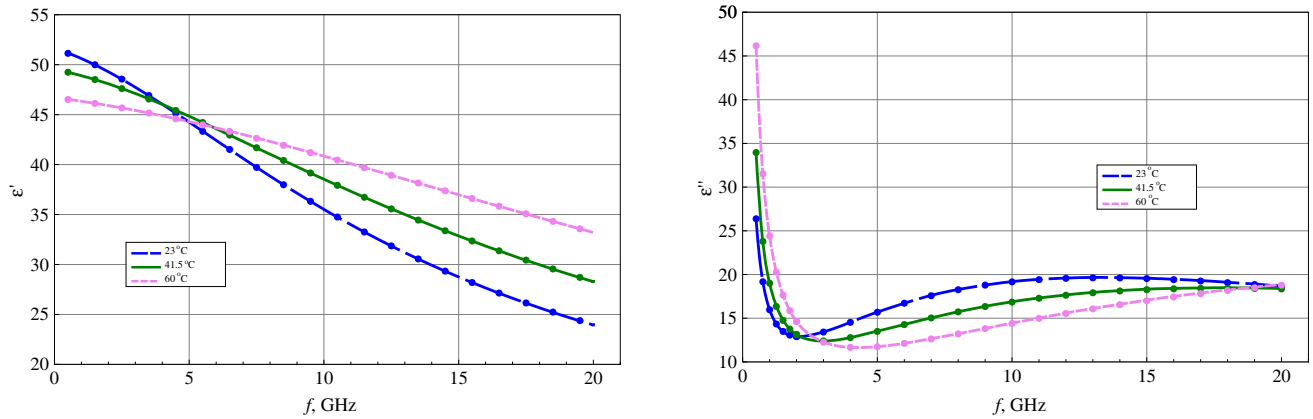

Figure 9. Dielectric properties ε', ε'' of animal liver at three different temperatures based on the approximations from Section 4.5 (solid lines), and the results reported in [24] (dots).

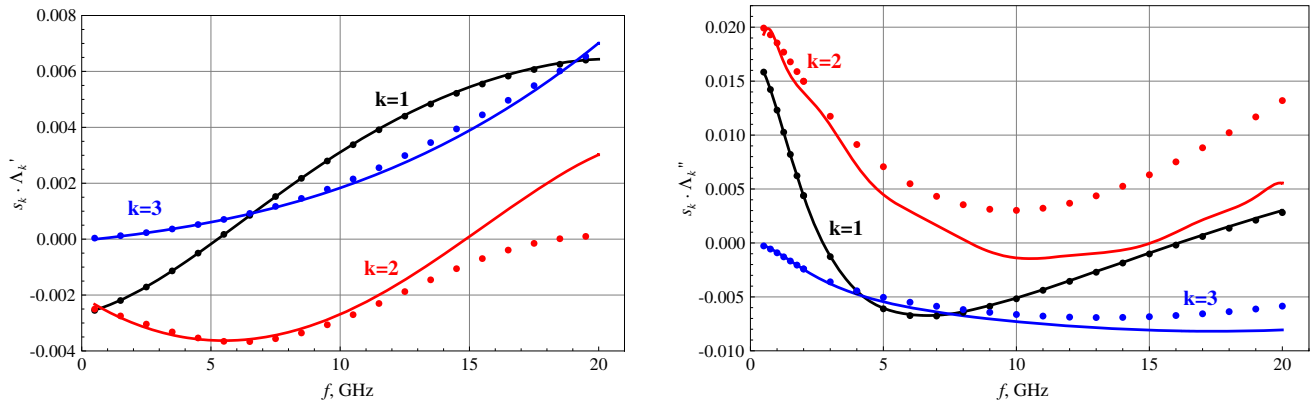

Figure 10. Temperature coefficients for the complex dielectric permittivity of animal liver based on Eq. (3.3) and the approximations from Section 4.5 (solid lines), and on the power series approximation (3.5) (dots), for $T_r = T_m$. The scaling coefficient s_k is 1 for $k = 1$, 10^2 for $k = 2$, and 10^3 for $k = 3$.

ε'': $L = 2$, $r = 0.20\%$,

$$\begin{aligned} b_0 &= 23.28048 + 6.093682\mathfrak{T}_1(x) + 1.75161\mathfrak{T}_2(x) - 1.9565\mathfrak{T}_3(x) + 1.17338\mathfrak{T}_4(x) \\ &\quad -0.57987\mathfrak{T}_5(x) + 0.33479\mathfrak{T}_6(x) - 0.19322\mathfrak{T}_7(x) + 0.11148\mathfrak{T}_8(x) \\ &\quad -0.064319\mathfrak{T}_9(x) + 0.037111\mathfrak{T}_{10}(x) - 0.021414\mathfrak{T}_{11}(x) + 0.012358\mathfrak{T}_{12}(x) \\ &\quad -0.018733\mathfrak{T}_{13}(x) + 0.010796\mathfrak{T}_{14}(x) - 0.0062229\mathfrak{T}_{15}(x), \end{aligned} \tag{4.20}$$

$$\begin{aligned} b_1 &= -0.18037 - 0.42486\mathfrak{T}_1(x) + 0.16280\mathfrak{T}_2(x) - 0.063201\mathfrak{T}_3(x) + 0.03421\mathfrak{T}_4(x) \\ &\quad -0.024517\mathfrak{T}_5(x) + 0.01403\mathfrak{T}_6(x) - 0.0080412\mathfrak{T}_7(x) + 0.0046142\mathfrak{T}_8(x) \\ &\quad -0.0026501\mathfrak{T}_9(x) + 0.0015231\mathfrak{T}_{10}(x) - 0.00087587\mathfrak{T}_{11}(x) + 0.0005039\mathfrak{T}_{12}(x), \end{aligned} \tag{4.21}$$

$$10^3 \cdot b_2 = 3.1373 + 1.1602\mathfrak{T}_1(x) - 0.19031\mathfrak{T}_2(x) - 0.15711\mathfrak{T}_3(x) + 0.10862\mathfrak{T}_4(x). \tag{4.22}$$

4.5. Animal Liver [24, Table 2]

ε': $L = 3$, $r = 0.19\%$,

$$\begin{aligned} b_0 &= 28.5631 - 22.6298\mathfrak{T}_1(x) + 2.05503\mathfrak{T}_2(x) + 0.3170\mathfrak{T}_3(x) \\ &\quad -0.3761\mathfrak{T}_4(x) + 0.09142\mathfrak{T}_5(x), \end{aligned} \tag{4.23}$$

$$
\begin{aligned}
b_1 &= 0.5625 + 0.5742\mathfrak{T}_1(x) - 0.01597\mathfrak{T}_2(x) + 0.01089T_3(x) \\
&\quad +0.006065\mathfrak{T}_4(x) - 0.001617\mathfrak{T}_5(x), && (4.24)\\
\cdot b_2 &= -0.01129 - 0.01114\mathfrak{T}_1(x) - 0.001192\mathfrak{T}_2(x) - 0.0002214\mathfrak{T}_3(x), && (4.25)\\
10^4 \cdot b_3 &= 0.8613 + 0.9930\mathfrak{T}_1(x) + 0.1295\mathfrak{T}_2(x). && (4.26)
\end{aligned}
$$

ε'': $L = 3$, $r = 0.46\%$,

$$
\begin{aligned}
b_0 &= 25.46991 + 5.77835\mathfrak{T}_1(x) - 2.76428\mathfrak{T}_2(x) - 0.67156\mathfrak{T}_3(x) \\
&\quad +1.4388\mathfrak{T}_4(x) - 1.30002\mathfrak{T}_5(x) + 0.96666\mathfrak{T}_6(x) - 0.69354\mathfrak{T}_7(x) \\
&\quad +0.50046\mathfrak{T}_8(x) - 0.36365\mathfrak{T}_9(x) + 0.26481\mathfrak{T}_{10}(x) - 0.19282\mathfrak{T}_{11}(x) \\
&\quad +0.069318\mathfrak{T}_{12}(x) - 0.050467\mathfrak{T}_{13}(x) + 0.03673\mathfrak{T}_{14}(x) - 0.026726\mathfrak{T}_{15}(x) \\
&\quad +0.019443\mathfrak{T}_{16}(x) - 0.014143\mathfrak{T}_{17}(x) + 0.010286\mathfrak{T}_{18}(x) - 0.024804\mathfrak{T}_{19}(x) \\
&\quad +0.018032\mathfrak{T}_{20}(x) - 0.013109\mathfrak{T}_{21}(x), && (4.27)\\
b_1 &= -0.58475 - 0.32518\mathfrak{T}_1(x) + 0.14023\mathfrak{T}_2(x) - 0.040014\mathfrak{T}_3(x) \\
&\quad +0.013128\mathfrak{T}_4(x) - 0.0013986\mathfrak{T}_5(x) - 0.00011555\mathfrak{T}_6(x) \\
&\quad -0.00020656\mathfrak{T}_7(x) + 0.00032556\mathfrak{T}_8(x) - 0.00027024\mathfrak{T}_9(x) \\
&\quad +0.00019287\mathfrak{T}_{10}(x) - 0.000135\mathfrak{T}_{11}(x) + 0.0038954\mathfrak{T}_{12}(x) \\
&\quad -0.0028309\mathfrak{T}_{13}(x) + 0.0020575\mathfrak{T}_{14}(x) - 0.0014954\mathfrak{T}_{15}(x) \\
&\quad +0.0010869\mathfrak{T}_{16}(x) - 0.00079003\mathfrak{T}_{17}(x) + 0.00057425\mathfrak{T}_{18}(x), && (4.28)\\
b_2 &= 0.013778 + 0.0074208\mathfrak{T}_1(x) - 0.001291\mathfrak{T}_2(x) - 0.00063344\mathfrak{T}_3(x) \\
&\quad +0.00048347\mathfrak{T}_4(x) - 0.00041738\mathfrak{T}_5(x) + 0.00031699\mathfrak{T}_6(x) \\
&\quad -0.00022857\mathfrak{T}_7(x) + 0.00016446\mathfrak{T}_8(x) - 0.00011913\mathfrak{T}_9(x) \\
&\quad +0.000086578\mathfrak{T}_{10}(x) - 0.000062962\mathfrak{T}_{11}(x), && (4.29)\\
10^4 \cdot b_3 &= -1.0162 - 0.70134\mathfrak{T}_1(x) + 0.23338\mathfrak{T}_2(x). && (4.30)
\end{aligned}
$$

5. SUMMARY

In this paper, we have presented the use of the bivariate Chebyshev series to generate polynomial approximations for the frequency and temperature dependent dielectric functions of materials. This technique has enabled us to provide simple polynomial approximations with a relative error less than 1% of the experimental wideband temperature-dependent dielectric functions described in [24, 25], for the biological tissues studied.

The Chebyshev series technique has allowed us to represent the temperature coefficients in the form of rational functions of frequency, in contrast with the power series approach, where the temperature coefficients are obtained as the derivatives of the exact dielectric functions with respect to the temperature variable. Numerical experiments have shown that we gain improved accuracy and need fewer temperature coefficients by employing the framework of the Chebyshev series approximation for the dielectric functions, as compared to using the power series approach.

The algorithm allows a straightforward extension to the case where the dielectric functions depend on more than the two variables, f and T.

A complete model of the EM properties of *living* tissues must include *the local blood flow* (LBF) as an independent variable. From physical perspective, a biotissue can be regarded as a mixture of several substances, including blood, which differ in their EM properties. Due to high permittivity of blood at microwave frequencies, the variations in the LBF may cause the EM properties of the mixture to change. The blood perfusion may vary as a result of a thermally induced vasodilation or vasoconstriction of the local blood vessels — e.g., see [30]. As was experimentally shown in [31], the LBF exhibits a barely discernible increase with local temperatures below a certain critical value ($\sim 41.5^\circ$C), and shows a rapid (and practically linear) increase with temperatures above the critical value. However, many data for biotissues have been estimated only from the *ex vivo* studies where the blood flow is difficult to realize or control. This experimental problem can be resolved by perfusing an excised tissue sample with natural

or artificial blood using a pump. Alternatively, the effective permittivity of a perfused tissue can be estimated using a mixing rule approach [32].

A prominent feature of many biotissues is that they demonstrate spatial inhomogeneity on many scales [33]. The measurement of the EM response of such a multi-scale composite medium yields the smoothed, averaged value over the inhomogeneities whose sizes are much smaller then the size of the receiving aperture (for definiteness, we here mean the open-ended waveguide measurement method). This may introduce a dependence of the experimental results upon the size of the field-probe interaction region (i.e., the aperture diameter) even if the size and mass of the tissue sample are sufficiently large so that the model of an infinite medium under test applies.

ACKNOWLEDGMENT

The authors are indebted to Eric Lemay (Consumer and Clinical Radiation Protection Bureau, Ottawa) for valuable improvements of the text. They owe the discussion in Section 5 of the parameters affecting the measured permittivity values to the anonymous referee whose comments are gratefully acknowledged.

APPENDIX A. CONVERGENCE OF THE POWER SERIES FOR THE TEMPERATURE-DEPENDENT COLE-COLE MODELS

In the Kth-order Cole-Cole model, the real part ε' and the imaginary part ε'' of the complex relative permittivity are given by [16, Eq. (7)]:

$$\varepsilon' = \varepsilon_\infty + \sum_{k=1}^{K} \frac{\Delta\varepsilon_k}{D_k} \left(1 + x_k \sin\frac{\pi\alpha_k}{2}\right), \tag{A1}$$

$$\varepsilon'' = \sum_{k=1}^{K} \frac{\Delta\varepsilon_k}{D_k} x_k \cos\frac{\pi\alpha_k}{2} + \frac{a_S}{2\pi f}, \tag{A2}$$

$$D_k = 1 + 2x_k \sin\frac{\pi\alpha_k}{2} + x_k^2, \tag{A3}$$

$$x_k = (2\pi f\tau_k)^{1-\alpha_k}. \tag{A4}$$

Here, the following real-valued quantities are involved: ε_∞ is the infinite-frequency relative permittivity; $\Delta\varepsilon_k$ are the dispersion amplitudes; τ_k ($\tau_k > 0$) are the relaxation times, α_k ($0 \le \alpha_k < 1$) are the exponents; a_S determines the static conductivity; and f ($f > 0$), as before, is the cyclic frequency. Putting all α_k's to 0, one obtains the Debye model. For the temperature-dependent model, the parameters ε_∞, $\Delta\varepsilon_k$, τ_k, a_S are taken as (non-zero) real polynomials in the temperature variable T [22, 24, 25], with $\tau_k(T)$ being non-constant ($\deg\tau_k \ge 1$) and positive on $[T_{\min}, T_{\max}]$.

To gain insight into the range of validity of the power series expansions of $\varepsilon'(f,T)$, $\varepsilon''(f,T)$ in the temperature variable, we shall now view T as the complex variable, and extend $\varepsilon'(f,T)$, $\varepsilon''(f,T)$ into the complex T-domain by analytically continuing Eqs. (A1)–(A4) and the appertaining polynomial expressions for the Cole-Cole parameters $\varepsilon_\infty(T)$, $\Delta\varepsilon_k(T)$, $\tau_k(T)$, $a_S(T)$.

The complex functions $\varepsilon'(f,T)$, $\varepsilon''(f,T)$ are regular everywhere in the complex T-plane except for the isolated singularities of the summands within the summation over k ($k = 1, 2, \ldots, K$). Note that the k-th summands in Eq. (A1) and Eq. (A2) have the same singularities. Since we do not need the Debye model, hereafter it is assumed that $0 < \alpha_k < 1$ for all k. Then the k-th summand is a multivalued function of T due to the presence of the complex power function $\tau_k^{1-\alpha_k}(T)$. Let us consider the zeros of the polynomial $\tau_k(T)$,

$$\tau_k(T) = 0. \tag{A5}$$

We shall assume that all zeros of $\tau_k(T)$ are simple, as is the case with the experimental polynomials from [24, 25]. Then every such zero is a branch point of the function $\tau_k^{1-\alpha_k}(T)$, and no other point in the finite T plane can be a branch point of the latter [34, Sec. 55, pp. 219–224; Sec. 57, p. 229]. We shall

resolve this function into single-valued branches by extending the branch cuts from each branch point to infinity along the multi-connected curve $T = T_k(u)$ which is defined implicitly by an equation

$$\tau_k(T) = -iu, \quad (0 \le u < +\infty). \tag{A6}$$

To fix the a definite single-valued branch of $\tau_k^{1-\alpha_k}(T)$, it is sufficient to restrict the argument of $\tau_k(T)$ by

$$-\frac{\pi}{2} + 2\pi p_k < \arg \tau_k(T) \le \frac{3\pi}{2} + 2\pi p_k, \tag{A7}$$

where p_k is an integer. In the practically important case where α_k is a rational number, it can be expressed in a unique way as a fraction q_k/r_k of two coprime natural numbers q_k, r_k such that $r_k \ge q_k+1$. Then there are just r_k distinct branches, and it suffices to take [34, Sec. 57, p. 231]

$$p_k = 0, 1, 2, \ldots, r_k - 1 \tag{A8}$$

to enumerate all these branches. Once a single-valued branch of $\tau_k^{1-\alpha_k}(T)$ $(k = 1, 2, \ldots, K)$ has been defined, it leads in an natural way to the definition of the corresponding single-valued branches for the k-th summand and other related functions. Obviously, the branches of $\varepsilon_r'(f,T)$, $\varepsilon_r''(f,T)$ on the slit T-plane can be uniquely enumerated by the multi-index $(p_1, p_2, \ldots, p_K)$, with the principal branches which agree with Eqs. (A1)–(A2) on $[T_{\min}, T_{\max}]$ being determined by $p_1 = p_2 = \ldots = p_K = 0$.

We are now in a position to consider the poles of the k-th summand. These poles arise as the zeros of the denominator $D_k(T)$. For simplicity, we exclude from the consideration a possibility that such zero is canceled out by the same zero of $\Delta\varepsilon_k(T)$ in the numerator. It is easy to see that $T = T_{\text{pole}}(f)$ is a zero of the p_k-th branch of $D_k(T)$ iff either

(i) there exists an integer n such that

$$p_k(1-\alpha_k) - \frac{1}{2} < n \le p_k(1-\alpha_k) - \alpha_k + \frac{1}{2} \tag{A9}$$

and T_{pole} is a root of the polynomial equation

$$\tau_k(T) = \frac{1}{2\pi f}\, e^{i\pi\left(\frac{2n+1}{1-\alpha_k} - \frac{1}{2}\right)}, \tag{A10}$$

or

(ii) there exists an integer n such that

$$-p_k(1-\alpha_k) - 1 + \frac{\alpha_k}{2} \le n < -p_k(1-\alpha_k) - \frac{\alpha_k}{2}, \tag{A11}$$

and T_{pole} is a root of the polynomial equation

$$\tau_k(T) = \frac{1}{2\pi f}\, e^{-i\pi\left(\frac{2n+1}{1-\alpha_k} - \frac{1}{2}\right)}. \tag{A12}$$

The restrictions in Eqs. (A9), (A11) on the values of the integer parameter n have been obtained from Eq. (A7). Each of the double inequalities in Eqs. (A9), (A11) has at most one solution, n. Accordingly, the p_k-th branch of the k-th summand may have no more than $2\deg\tau_k$ poles.

If the principal branch of $\nu(f,T) = \varepsilon_r'(f,T), \varepsilon_r''(f,T)$ is regular at some point T_r, then it can be developed as a power series in T around T_r, and the radius of convergence of the series is equal to the distance from T_r to the nearest singularity — a branch point or a pole — of $\nu(f,T)$ in the complex T-domain [34, Sec. 84, p. 385, Thm. 17.10, pp. 391–394]. Since ε_r' and ε_r'' in Eqs. (A1), (A2) have the same singularities, the radius (but not necessarily the rate) of convergence is the same for both series. For the temperature-dependent Cole-Cole models of [24, 25], and T_r set to the average measured temperature in Eq. (1.9), any poles of $\nu(f,T)$ for all measured frequencies in Eq. (1.5) lie much farther away from T_r than the branch points. The radii of convergence of the appertaining power series are summarized in Table A1. Interestingly, they are the same for all frequencies because the location of the branch points does not depend upon f.

Table A1. Radius of convergence R_T of the power series expansions in T about the point T_r for some experimental temperature-dependent Cole-Cole functions $\varepsilon'(f,T), \varepsilon''(f,T)$.

Tissue	Liver [24]	Liver [25]	Muscle [25]	Fat [25]	Blood [25]
R_T, °C	36.0	49.5	48.5	24.9	41.1
$\frac{1}{2}\Delta T$, °C	18.5	10	10	10	10
T_r, °C	41.5	40	40	40	40

REFERENCES

1. Klemm, M. and G. Troester, "EM energy absorption in the human body tissues due to UWB antennas," *Progress In Electromagnetics Research*, Vol. 62, 261–280, 2006.
2. Hirata, A., T. Asano, and O. Fujiwara, "FDTD analysis of human body-core temperature elevation due to RF far-field energy prescribed in the ICNIRP guidelines," *Phys. Med. Biol.*, Vol. 52, No. 16, 5013–5023, Aug. 21, 2007.
3. Foster, K. R., M. C. Ziskin, and Q. Balzano, "Thermal response of human skin to microwave energy: A critical review," *Health Phys.*, Vol. 111, No. 6, 528–541, Dec. 2016.
4. Rotman, R., "Recent advances using microwaves for imaging, hyperthermia and interstitial ablation of breast cancer tumors," *Proc. IEEE Int. Conf. Microw. Commun. Antennas Electron. Syst. (COMCAS)*, 1–4, Tel Aviv, Israel, Nov. 7–9, 2011.
5. Vrbova, B. and J. Vrba, "Microwave thermotherapy in cancer treatment: Evaluation of homogeneity of SAR distribution," *Progress In Electromagnetics Research*, Vol. 129, 181–195, 2012.
6. Nguyen, P. T., A. Abbosh, and C. Crozier, "Three-dimensional microwave hyperthermia for breast cancer treatment in a realistic environment using particle swarm optimization," *IEEE Trans. Biomed. Eng.*, Vol. 64, No. 6, 1335–1344, Jun. 2017.
7. Kim, T.-H. and J.-K. Pack, "Measurement of electrical characteristics of female breast tissues for the development of the breast cancer detector," *Progress In Electromagnetics Research C*, Vol. 30, 189–199, 2012.
8. Fiser, O., M. Helbig, J. Sachs, S. Ley, I. Merunka, and J. Vrba, "Microwave non-invasive temperature monitoring using UWB radar for cancer treatment by hyperthermia," *Progress In Electromagnetics Research*, Vol. 162, 1–14, 2018.
9. Yilmaz, T., R. Foster, and Y. Hao, "Radio-frequency and microwave techniques for non-invasive measurement of blood glucose levels," *Diagnostics (Basel)*, Vol 9, No. 1, Article No. 6, 1–34, Jan. 8, 2019.
10. Chandrasekaran, S., S. Ramanathan, and T. Basak, "Microwave food processing — A review," *Food Res. Int.*, Vol. 52, No. 1, 243–261, Jun. 2013.
11. Keshavarz, R., M. Danaeian, M. Movahhedi, and A. Hakimi, "A compact dual-band branch-line coupler based on the interdigital transmission line," *19th Iranian Conf. Electr. Eng.*, 1–5, Tehran, Iran, May 17–19, 2011.
12. Keshavarz, R., Y. Miyanaga, M. Yamamoto, T. Hikage, and N. Shariati, "Metamaterial-inspired quad-band notch filter for LTE band receivers and WPT applications," *33rd GA & Sci. Symp. Int. Union Rad. Sci.*, 1–4, Rome, Italy, Aug. 29–Sep. 5, 2020.
13. Keshavarz, R. and N. Shariati, "Low profile metamaterial band-pass filter loaded with 4-turn complementary spiral resonator for WPT applications," *27th IEEE Int. Conf. Electron., Circ. Syst. (ICECS)*, 1–4, Glasgow, UK, Nov. 23–25, 2020.
14. Keshavarz, S., R. Keshavarz, and A. Abdipour, "Compact active duplexer based on CSRR and interdigital loaded microstrip coupled lines for LTE application," *Progress In Electromagnetics Research C*, Vol. 109, 27–37, 2021.
15. Debye, P., "Zur Theorie der spezifischen Wärmen," *Ann. Phys.*, Vol. 344, No. 14, (B. 39, F. 4), 789–839, 1912.

16. Cole, K. S. and R. H. Cole, "Dispersion and absorption in dielectrics. I. Alternating current characteristics," *J. Chem. Phys.*, Vol. 9, No. 4, 341–351, Apr. 1941.
17. Gabriel, S., R. W. Lau, and C. Gabriel, "The dielectric properties of biological tissues: III. Parametric models for the dielectric spectrum of tissues," *Phys. Med. Biol.*, Vol. 41, No. 11, 2271–2293, Nov. 1996.
18. Krewer, F., F. Morgan, and M. O'Halloran, "Development of accurate multi-pole Debye functions for electromagnetic tissue modelling using a genetic algorithm," *Progress In Electromagnetics Research Letters*, Vol. 43, 137–147, 2013.
19. Salahuddin, S., E. Porter, F. Krewer, and M. O'Halloran, "Optimized analytical models of the dielectric properties of biological tissue," *Med. Eng. Phys.*, Vol. 43, 103–111, May 2017.
20. Trujillo, M. and E. Berjano, "Review of the mathematical functions used to model the temperature dependence of electrical and thermal conductivities of biological tissue in radiofrequency ablation," *Int. J. Hypertherm.*, Vol. 29, No. 6, 590–597, 2013.
21. Rossmann, C. and D. Haemmerich, "Review of temperature dependence of thermal properties, dielectric properties, and perfusion of biological tissues at hyperthermic and ablasion temperatures," *Crit. Rev. Biomed. Eng.*, Vol. 42, No. 6, 467–492, 2014.
22. Jaspard, F. and M. Nadi, "Dielectric properties of blood: An investigation of temperature dependence," *Physiol. Meas.*, Vol. 23, No. 3, 547–554, Jul. 2002.
23. Wolf, M., R. Gulich, P. Lunkenheimer, and A. Loidl, "A broadband dielectric spectroscopy on human blood," *Biochim. Biophys. Acta Gen. Subj.*, Vol. 1810, No. 8, 727–740, Aug. 2011.
24. Lazebnik, M., M. C. Converse, J. H. Booske, and S. C. Hagness, "Ultrawideband temperature-dependent dielectric properties of animal liver tissue in the microwave frequency range," *Phys. Med. Biol.*, Vol. 51, No. 7, 1941–1955, Apr. 7, 2006.
25. Ley, S., S. Shilling, O. Fiser, J. Vrba, J. Sachs, and M. Helbig, "Ultra-wideband temperature dependent dielectric spectroscopy of porcine tissue and blood in the microwave frequency range," *Sensors (Basel)*, Vol. 19, No. 7, Article No. 1707, 1–21, 2019.
26. Mason, J. C. and D. C. Handscomb, *Chebyshev Polynomials*, Chapman & Hall/CRC, Boca Raton, FL, 2003.
27. Mason, J. C., "Near-best multivariate approximation by Fourier series, Chebyshev series and Chebyshev interpolation," *J. Approx. Theory*, Vol. 28, No. 4, 349–358, Apr. 1980.
28. Trefethen, L. N., "Multivariate polynomial approximation in the hypercube," *Proc. Amer. Math. Soc.*, Vol. 145, No. 11, 4837–4844, Nov. 2017.
29. Taflove, A., *Computational Electrodynamics. The Finite-Difference Time-Domain Method*, Artech House, Boston, MA, 1995.
30. McGarr, G. W., "Influence of upper limb ischaemia-reperfusion injury on the regulation of cutaneous blood flow during local hyparaemia," PhD diss., Brock Univ., St. Catharines, ON, Canada, 2017.
31. Sekins, K. M., J. F. Lehmann, P. Esselmann, D. Dundore, A. F. Emery, B. J. de Lateur, and W. B. Nelp, "Local muscle blood flow and temperature responses to 915 MHz diathermy as simultaneously measured and numerically predicted," *Arch. Phys. Med. Rehabil.*, Vol. 65, No. 1, 1–7, Jan. 1984.
32. Sihvola, A., "Mixing rules with complex dielectric coefficients," *Subsurf. Sens. Tech. App.*, Vol. 1, No. 4, 393–415, 2000.
33. Porter, E., A. L. Gioia, A. Santorelli, and M. O'Halloran, "Modeling of the dielectric properties of biological tissues within the histology region," *IEEE Trans. Dielectr. Electr. Insul.*, Vol. 24, No. 5, 3290–3301, Oct. 2017.
34. Markushevich, A. I., *Theory of Functions of a Complex Variable*, Vol. 1, Transl. R. A. Silverman, Prentice-Hall, Englewood Cliffs, NJ, 1965.